separations

MDPI

Article

In Situ XRD, Raman Characterization, and Kinetic Study of CO_2 Capture by Alkali Carbonate-Doped Na_4SiO_4

Zhen Wang, Chenteng Sun *, Qian Xu *, Xingli Zou, Hongwei Cheng and Xionggang Lu

School of Materials Science and Engineering, Shanghai University, Shanghai 200072, China
* Correspondence: sunchenteng@shu.edu.cn (C.S.); qianxu@shu.edu.cn (Q.X.)

Abstract: Sodium silicate, a new type of CO_2 sorbent, has a relatively low cost, but its sorption reactivity is not yet good enough. Alkali carbonate doping is commonly used as an effective means to improve the CO_2 uptake reactivity of solid sorbents. In this study, sodium orthosilicate, Na_4SiO_4, was synthesized and mixed with 5, 10, and 20 mol% of Li_2CO_3–Na_2CO_3 or Li_2CO_3–Na_2CO_3–K_2CO_3 as CO_2 sorbents. The promotion of alkali carbonates on Na_4SiO_4 in CO_2 capture was characterized using thermal analyses in an 80 vol% CO_2–20 vol% N_2 atmosphere. The phase evolution and structural transformations during CO_2 capture were characterized by in situ XRD and Raman, and the results showed that the intermediate pyrocarbonate, $C_2O_5^{2-}$, which emerged from alkali carbonates, enhanced the CO_2 capture of Na_4SiO_4 to form Na_2CO_3 and Na_2SiO_3 from 100 °C. Isothermal analyses showed that 10 mol% of Li_2CO_3–Na_2CO_3 was the optimal additive for Na_4SiO_4 to attain better CO_2 uptake performance. The alkali carbonates were effective in reducing the activation energy for both chemisorption and bulk diffusion, improving the cycle stability of Na_4SiO_4.

Keywords: CO_2 capture; Na_4SiO_4; alkali carbonates; in situ XRD; in situ Raman; isothermal analysis; double exponential model; Eyring's model

Citation: Wang, Z.; Sun, C.; Xu, Q.; Zou, X.; Cheng, H.; Lu, X. In Situ XRD, Raman Characterization, and Kinetic Study of CO_2 Capture by Alkali Carbonate-Doped Na_4SiO_4. *Separations* **2022**, *9*, 428. https://doi.org/10.3390/separations9120428

Academic Editor: Federica Raganati

Received: 15 November 2022
Accepted: 8 December 2022
Published: 10 December 2022

1. Introduction

CO_2 emissions have become a world concern due to their huge impact on global warming [1,2]. CO_2 capture and storage (CCS) technology using different amine solvents or solid chemisorbents has been proposed as the most promising method for the removal of CO_2 from industrial flue gases [3,4]. Among CO_2 captors, Monoethanolamine (MEA) and diethanolamine (DEA) are representative amine solvents used for CO_2 capture, but high cost, energy loss, and corrosiveness plague their widespread application [5,6]. Solid sorbents such as CaO [6,7] or MgO [8,9] seem to be optional CO_2 captors due to their low cost and good reactivity. However, the dense solid product layer covering the unreacted sorbents restricts CO_2 diffusion and further reaction. Some alkali ceramics also have the potential to be CO_2 sorbents due to desirable properties, including good selectivity, sorption capacity, and proper kinetics for CO_2 capture [10]. Alkaline ceramics such as Li_2ZrO_3 [11,12], Na_2ZrO_3 [13,14], Li_3BO_3 [15,16], $NaBO_2$ [17,18], $LiYO_2$ [19], $NaYO_2$ [19], and Li_4SiO_4 [20–22] have been studied as potential CO_2 captors because they can work at high temperatures with good CO_2 uptake capacity. Among these alkali ceramics, Li_4SiO_4 has attracted more attention because of its relatively better CO_2 capture reactivity and durability. However, high raw material prices seem to be the limiting factor for Li_4SiO_4 in large-scale applications [23]. Therefore, it is desired to develop low-cost alternative materials with good CO_2 capture performance.

Some studies [23–29] on CO_2 capture by chemisorption have been performed using sodium silicates, which may be alternatives to Li_4SiO_4. It is worth studying whether Na_4SiO_4 has the potential to be developed as a low-cost CO_2 sorbent, as well as how to reasonably improve its CO_2 uptake performance. Rodríguez [28] found that Na_2SiO_3 can achieve CO_2 capture at 80–120 °C, but the adsorption capacity was very low due to poor

kinetics. Sanna [23,26,27] prepared sodium-based silicates from fly ash and Na_2CO_3, and the main phases were Na_2SiO_3 and Na_4SiO_4, which exhibited better CO_2 sorption and desorption properties at 700 °C. This suggests that Na_4SiO_4 has better reactivity in CO_2 capture compared with Na_2SiO_3. In the previous study [24], it was found that the reaction of CO_2 with Na_4SiO_4 can be expressed as Equation (1). The CO_2 capture of Na_4SiO_4 took place from 200 °C with a minor weight gain rate until rapid chemisorption occurred above 750 °C. Although Na_4SiO_4 has a wider temperature window for CO_2 capture than Li_4SiO_4, it is necessary to take measures to enhance the CO_2 uptake of Na_4SiO_4 at different temperatures, thereby reducing energy consumption at different operating conditions.

$$CO_2(g) + Na_4SiO_4 \rightleftharpoons Na_2SiO_3 + Na_2CO_3 \quad (1)$$

It has been reported that CO_2 capture capacity can be improved by doping with molten salts, such as halides for CaO [6,7] and nitrates for MgO [8,9]. Alkali carbonate doping is also widely adopted as an accessible and facile method to improve the CO_2 uptake performance of moderate and high-temperature sorbents [24,25,30–33]. The facilitation of alkali carbonates in CO_2 capture is usually attributed to the eutectic melt produced from doped carbonates and products, allowing the CO_2 to diffuse in the liquid phase rather than solely in the solid phase. In addition to melt formation, carbonates can produce the pyrocarbonate $C_2O_5^{2-}$ to speed up CO_2 diffusion. Zhang [34] found that $C_2O_5^{2-}$ acted as an active species in molten alkali carbonates to accelerate CO_2 transport. Corradini [35] proposed that CO_2 diffusion in molten $CaCO_3$ took place through a Grotthuss-like mechanism via $C_2O_5^{2-}$, which was three times quicker than solely molecular diffusion of CO_2. In the previous study [24,25], it was confirmed that alkali carbonates were thermodynamically favorable for the CO_2 uptake of Na_4SiO_4 under an air atmosphere or 80 vol% CO_2–20 vol% N_2 because alkali carbonates could bind CO_2 to form $C_2O_5^{2-}$. This provided a new idea for alkali carbonates to promote CO_2 chemisorption of Na_4SiO_4 from 200 °C, apart from melt-accelerated CO_2 diffusion. However, when the mass ratio of Na_4SiO_4 and single carbonates was 1:0.5 [24], the proportion of Na_4SiO_4 in sorbents decreased, resulting in a lowered CO_2 adsorption capacity. Under air atmosphere, the CO_2 uptake performance of alkali Na_2CO_3-doped Na_4SiO_4 was also found to become progressively better when the content of Na_2CO_3 in the Na_4SiO_4-based sorbents was reduced from 66.7 wt% to 50 wt% and then to 33.3 wt% [25]. In light of this, the proportion of alkali carbonates in the sorbents must be appropriately reduced. Given that the contribution of carbonates includes the production of pyrocarbonates and melts, different single alkali carbonates should be reasonably combined to exert the promoting effect of carbonates corresponding to the solid or molten state at different temperatures. On the other hand, the enhanced CO_2 uptake kinetics of Na_4SiO_4 at different temperatures by pyrocarbonates and carbonate melts has not yet been discussed. Hence, it is required to fit the CO_2 uptake results using a kinetic model so that the positive roles of alkali carbonates can be assessed based on kinetic parameters. The double exponential model and Eyring's model are the most commonly used models for analyzing CO_2 uptake kinetics, which take into account two independent processes: surface chemisorption and bulk diffusion, and fit well with experimental data [14,36,37]. Then, the fitted kinetic results are estimated by Eyring's model to determine the activation energies of the different processes [14,38].

As a continuation of our previous work [24,25], here, Na_4SiO_4 will be synthesized and mixed with 5, 10, and 20 mol% of Li_2CO_3–Na_2CO_3 or Li_2CO_3–Na_2CO_3–K_2CO_3 as CO_2 sorbents. In situ XRD and Raman will be performed to characterize the phase evolution and structural transformations during the CO_2 uptake of alkali carbonates doped Na_4SiO_4. The CO_2 sorption properties will be investigated by isothermal analyses at different temperatures, and the CO_2 uptake kinetics will be evaluated by the double exponential model and Eyring's model. This study will focus on the contribution of pyrocarbonates that emerged from alkali carbonates in different species and amounted to the CO_2 uptake performance of Na_4SiO_4 at different temperatures.

2. Materials and Methods

2.1. Sorbents

The chemicals in this study, such as NaOH, $Na_2SiO_3 \cdot 9H_2O$, and alkali carbonates, were of analytical grade and bought from Aladdin Chemical Reagent Co., Ltd., Shanghai, China. Na_4SiO_4 was prepared by a wet mixing method using NaOH and $Na_2SiO_3 \cdot 9H_2O$ as the raw materials. Firstly, NaOH and $Na_2SiO_3 \cdot 9H_2O$ with a molar ratio of 2:1 were dissolved by de-ionized water in a 50 mL nickel crucible, and the solution was stirred for 1 h and dried in a vacuum drying oven at 100 °C for 24 h. Then, the powder was fired in a high-temperature furnace at 600 °C for 1 h under ambient air conditions, and blocky Na_4SiO_4 was obtained. After grinding, the Na_4SiO_4 powder was sieved and obtained with particles of 150–250 μm. Then, the binary carbonates Li_2CO_3–Na_2CO_3 and ternary carbonates Li_2CO_3–Na_2CO_3–K_2CO_3 at 28–48 μm were mixed with Na_4SiO_4 with different molar ratios of 5:95, 10:90, and 20:80; these sorbents were labeled as *x*(carbonates)*y*Na. For example, the sample named 10(LiNa)90Na refers to a mixture with a molar ratio of (Li_2CO_3–Na_2CO_3):Na_4SiO_4 = 10:90, while P–Na refers to pristine Na_4SiO_4. The doped binary carbonates or ternary carbonates were equimolarly mixed and pre-melted. The melting points of Li_2CO_3–Na_2CO_3 and Li_2CO_3–Na_2CO_3–K_2CO_3 are 500 °C and 393 °C [21], respectively.

2.2. Characterization

The X-ray powder diffraction patterns of the specimens were collected by a laboratory diffractometer (Bruker D8 ADVANCE, Bruker Inc., Karlsruhe, (Baden-Württemberg), Germany). The room temperature XRD data were collected in the range 2θ = 10–80 ° with a scan rate of $2^\circ \cdot min^{-1}$ at ambient atmosphere. In situ XRD characterization consists of two aspects: (1) the full-pattern scanning model in steps of 0.02 ° over the range 15–65 °. CO_2 chemisorption from 50 to 850 °C in an 80 vol% CO_2–20 vol% N_2 atmosphere with a heating step of 10 $°C \cdot min^{-1}$. When it was 850 °C, the temperature was held constant for 1 h, and the atmosphere switched to a 100 vol% N_2 atmosphere for desorption; (2) the characteristic peak range of 32.8–35.4 ° using the position-sensitive detector (PSD) fixed model, in which the experimental condition remained unchanged, and the heating rate was changed to 5 $°C \cdot min^{-1}$ from 50 °C to 850 °C. Desorption was performed under a 100 % N_2 atmosphere and accompanied by a cooling rate of 2 $°C \cdot min^{-1}$ from 850 °C to 50 °C. The gas flow rate was always 50 $mL \cdot min^{-1}$. The collected diffraction data of in situ XRD was refined by DIFFRAC.TOPAS5.0 software to determine the mass percentage of different phases in the samples at different temperatures.

In situ Raman spectra of different samples during CO_2 capture were measured using a laser confocal Raman spectrometer (LabRAM HR Evolution, Horiba France SAS, Villeneuve d'Ascq (Nord-Pas-de-Calais Region), France). A carrier table attached to the measurement system was used to load samples for in situ measurements from ambient temperature to 800 °C with a heating rate of 5 $°C \cdot min^{-1}$. The atmosphere composition and airflow size in the in situ Raman experiments were kept consistent with the experimental conditions described above.

The morphological features of the sorbents were characterized by scanning electron microscopy (SEM) using an FEI 450 (FEI, Hillsboro, NH, USA). To ensure visualization, a layer of platinum (thickness of 3–4 nm) was coated on the samples to enhance conductivity.

2.3. CO_2 Sorption

The CO_2 uptake performance of the sorbents was evaluated using a thermogravimetric analyzer (SDT650, TA Instrument, New Castle, DE, USA). Approximately 20 mg of the sample were loaded into a platinum crucible and heated from ambient temperature to 350 °C and held for 10 min under 100% N_2 at 50 $mL \cdot min^{-1}$ to remove moisture. Then, the temperature was changed to the targeted temperatures. Dynamic analyses were conducted from 50 to 900 °C under the 80% CO_2–20% N_2 atmosphere. Isothermal experiments for pristine and doped Na_4SiO_4 were carried out in two temperature ranges, 200–300 °C and 500–600 °C for 120 min. Since the focus of this study is on the promotion of Na_4SiO_4 by

alkali carbonates in CO_2 capture, 80 vol% CO_2 was selected to make the enhancement more significant and easily measured. Experiments with 20 consecutive cycles of CO_2 adsorption–desorption were performed at 600 °C with a flow of 80% CO_2 for adsorption (50 mL/min for 60 min) and 850 °C in pristine N_2 for desorption (50 mL/min for 90 min).

Since the theoretical weight gain of different samples will vary with the content of Na_4SiO_4, the conversion $\chi_{Na_4SiO_4}$ was proposed to describe the capture performance. The conversion $\chi_{Na_4SiO_4}$ was estimated according to Equation (2), in which Δm denotes the weight change before and after adsorption, m_0 denotes the theoretical capacity, x_n is the molar fraction of compositions, and M_n is the relative molecular weight of compositions.

$$\chi = \frac{\Delta m}{m_0} \times 100\% = \frac{\Delta m \times \Sigma(x_n \times M_n)}{M_{CO_2} \times \chi_{Na_4SiO_4}} \times 100\% \quad (2)$$

3. Results and Discussions

3.1. Characterization of the Prepared Na_4SiO_4

In this study, Na_4SiO_4 was prepared by a wet mixing method using NaOH and $Na_2SiO_3{\cdot}9H_2O$ as raw materials, heated from ambient temperature to 600 °C at a heating rate of 2 °C·min^{-1}, and it was maintained for 60 min. Figure 1a shows that the XRD plots of the prepared Na_4SiO_4 are consistent with the standard diffraction pattern of Na_4SiO_4 (JCPDSNo.78–1432). The results of XRD characterization suggested that the desired Na_4SiO_4 was successfully prepared. No typical peaks of impurities were detected, indicating that the NaOH and $Na_2SiO_3{\cdot}9H_2O$ could react adequately under the set synthetic conditions. The morphology of the prepared Na_4SiO_4 is shown in Figure 1b, presenting the cluster-shaped particles with a dense surface, as shown in the enlarged image. Additionally, there are obvious gaps in the distribution between the particles.

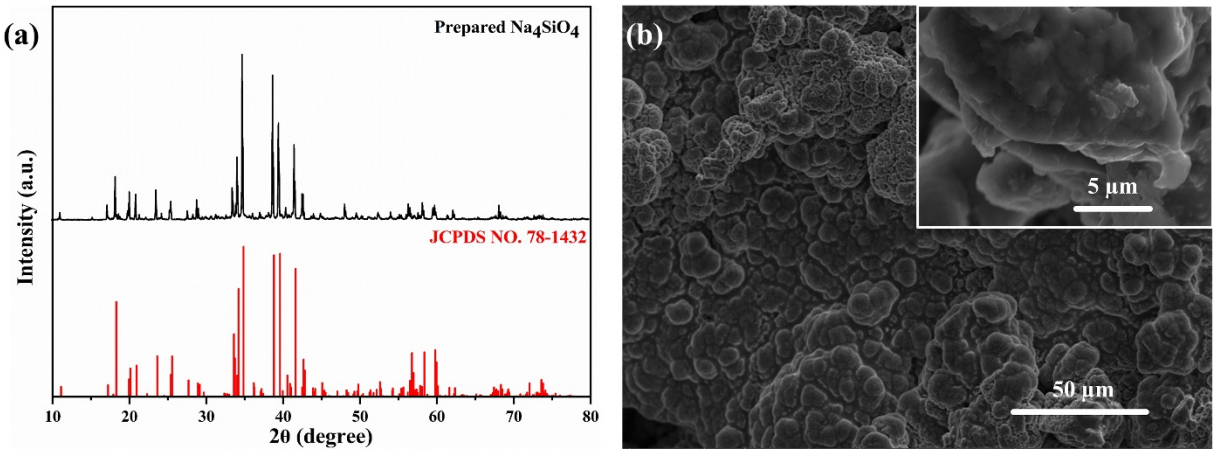

Figure 1. (**a**) XRD patterns and (**b**) SEM images of the Na4SiO4 synthesized at 600 °C.

3.2. In Situ XRD

To study the phase changes in CO_2 uptake of the P–Na, the in situ XRD plots of the P–Na were collected at 25–850 °C, as shown in Figure 2a. When it was 100 °C, only the Na_4SiO_4 phase was detected. When the temperature went up to 200 °C, the Na_2SiO_3 phase could be detected, which was the product of the carbonization reaction between Na_4SiO_4 and CO_2. When the temperature climbed to 400 °C, the Na_2CO_3 phase was found. The peak intensities of the Na_2SiO_3 and Na_2CO_3 phases gradually strengthened with increasing temperature, but the characteristic peak of Na_4SiO_4 was not found above 400 °C. From 400 to 800 °C, the dominant phases were Na_2SiO_3 and Na_2CO_3 during the CO_2 capture of Na_4SiO_4. In the mixture exposed to 80 vol% CO_2, the Na_2SiO_3 phase persisted after formation, and the SiO_2 phase was not found, implying that Na_2SiO_3 did not react with CO_2. This is different from the conclusion reported by Rodríguez [28] that Na_2SiO_3 can achieve CO_2 capture. When the temperature was up to 850 °C, the Na_2CO_3

phase vanished because 850 °C was approaching the melting point of Na_2CO_3, 860 °C. After that, the atmosphere was changed to 100% N_2 and kept for 60 min. Both the Na_2SiO_3 and Na_4SiO_4 phases were found, which indicated that desorption had not been completed under this condition.

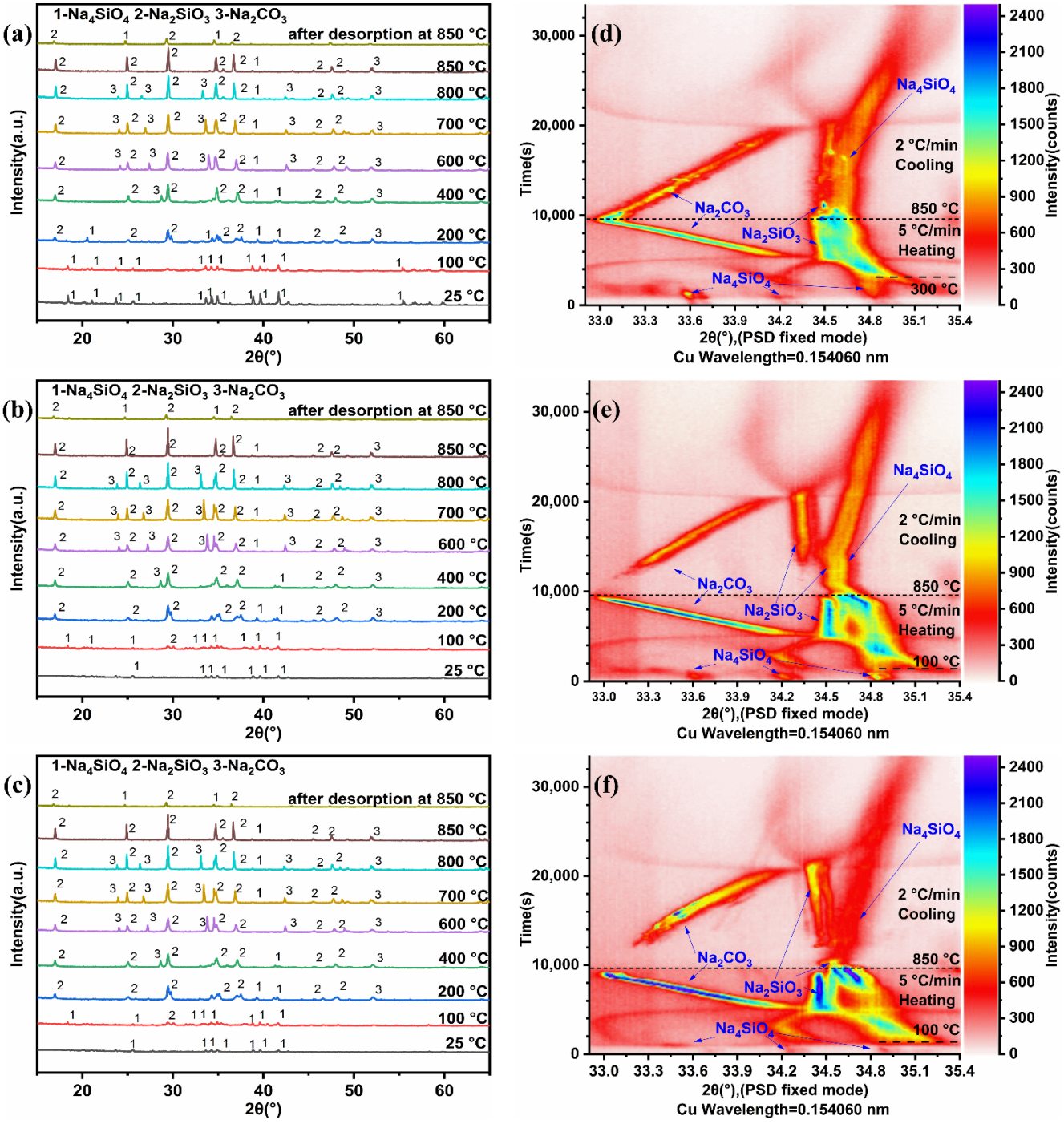

Figure 2. In situ XRD patterns of (**a**,**d**) P–Na, (**b**,**e**) 10(LiNa)90Na, and (**c**,**f**) 10(LiNaK)90Na at 25–850 °C in the 80 vol% CO_2–20% N_2 atmosphere; (**a**–**c**) in full-pattern scanning model over the range of 15–65° and (**d**–**f**) in the PSD model over the range of 32.8–35.4°.

To investigate the phase evolution of alkali carbonate-doped Na_4SiO_4 during CO_2 uptake, 10(LiNa)90Na and 10(LiNaK)90Na were used as representatives and characterized in the same temperature regime and atmosphere as described above, and their XRD plots are

shown in Figure 2b,c. It should be mentioned that when the mass percentage of a certain phase in the mixtures is less than 5 wt%, it is not detectable in the XRD measurement. This allowed us to exclude the interference of additives to the main phases, including Na_4SiO_4, Na_2SiO_3, and Na_2CO_3, during the study of phase transition. With the addition of carbonates, the Na_2SiO_3 phase was detected at 100 °C. As the temperature increased, the Na_4SiO_4 phase disappeared at 400 °C. When the temperature gradually increased to 800 °C, Na_2SiO_3 and Na_2CO_3 were the predominant phases, and no other miscellaneous phases were found. This indicated that alkali carbonates enhanced the CO_2 chemisorption of Na_4SiO_4 and did not change the direction of the reaction from the reactant, Na_4SiO_4, to the products, Na_2SiO_3 and Na_2CO_3. In addition, the mixed carbonates did not cause the reaction between Na_2SiO_3 and CO_2. After desorption at 850 °C for one hour, Na_2SiO_3 and Na_4SiO_4 phases were found, suggesting incomplete desorption despite the addition of carbonates. As shown in Figure 3, the mass percentage of different phases in in situ XRD characterization varies with temperature from 25 to 850 °C. For samples containing 10 mol% of Li_2CO_3–Na_2CO_3 or Li_2CO_3–Na_2CO_3–K_2CO_3, when the temperature rose to 200 °C, the mass fraction of the Na_4SiO_4 phase decreased rapidly to less than 5%, while Na_2SiO_3 and Na_2CO_3 increased rapidly and accounted for the majority at higher temperatures. In contrast, the same effect was only achieved at 600 °C for P–Na.

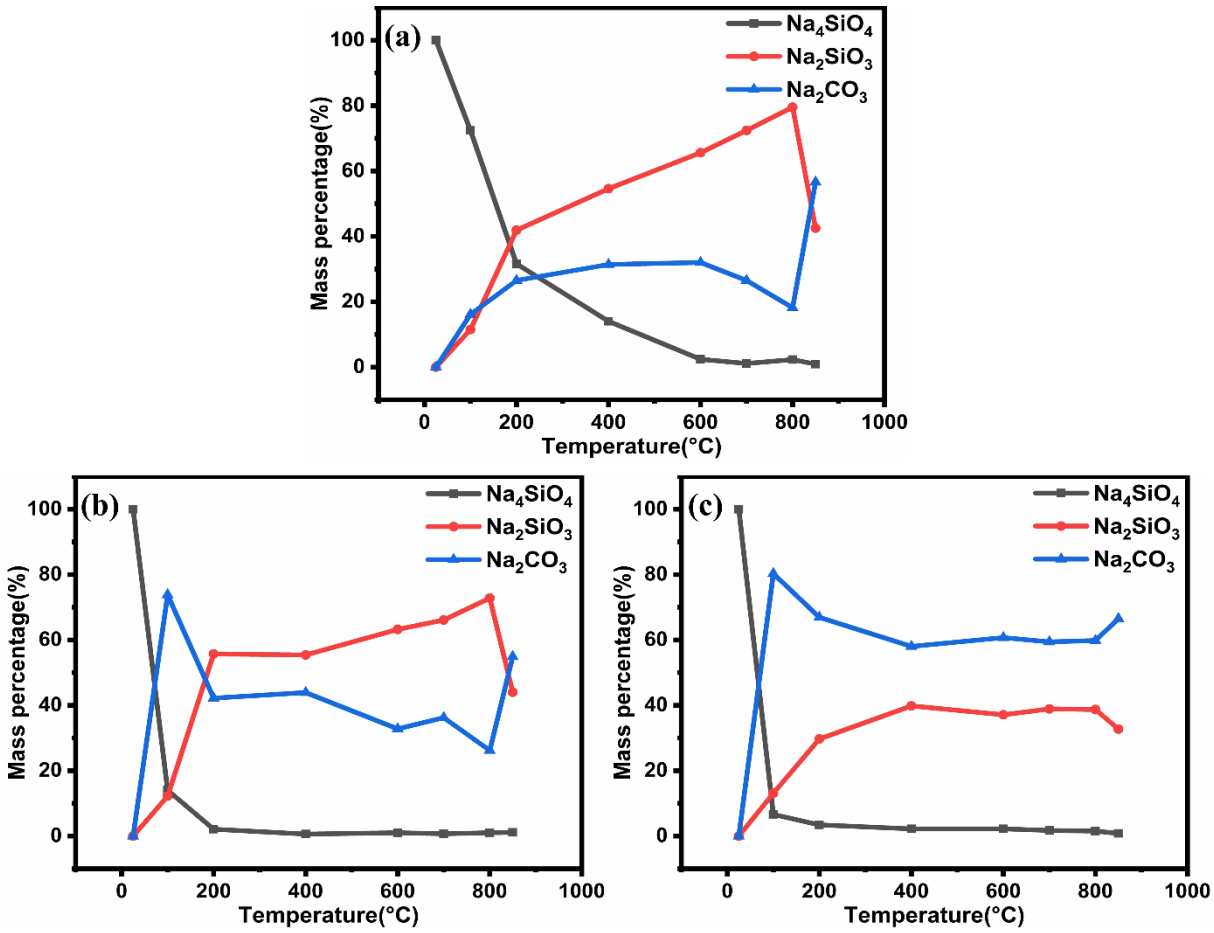

Figure 3. Mass percentage of different phases varying with temperature in in situ XRD characterization from 25 to 850 °C; (**a**) P–Na, (**b**) 10(LiNa)90Na, and (**c**) 10(LiNaK)90Na.

To further explore the CO_2 capture behavior of Na_4SiO_4 promoted by alkali carbonates, the collection of typic peaks in carbonation–decarbonization was recorded by in situ XRD using a position-sensitive detector (PSD) fixed model at the temperature range of 50–850 °C. The phase changes of P–Na are shown in Figure 2d. The sorbent was heated

in the 80 vol% CO_2–20 vol% N_2 atmosphere and cooled in 100% N_2 at the same flow rate, corresponding to different ramping rates of 5 °C·min^{-1} and 2 °C·min^{-1}, respectively. Figure 2e,f represents the continuous phase changes of 10(LiNa)90Na and 10(LiNaK)90Na at the same temperature and atmosphere regime. The carbonation and decarbonization processes are discussed specifically below:

Carbonization: In Figure 2d, the Na_2SiO_3 phase appeared at 300 °C. After which, the Na_4SiO_4 phase disappeared quickly with the increasing temperature. From 300 °C to 850 °C, the Na_2SiO_3 phase appeared in abundance with Na_2CO_3. As the temperature increased, the intensities of Na_2CO_3 and Na_2SiO_3 increased slowly. In Figure 2e,f, due to the addition of carbonates, the phase of Na_4SiO_4 vanished gradually at 100 °C. Hence, it was confirmed that the alkali carbonates allowed the CO_2 capture of Na_4SiO_4 to occur at lower temperatures. Under the same experimental conditions, for samples 10(LiNa)90Na and 10(LiNaK)90Na, the intensities of the Na_2CO_3 and Na_2SiO_3 phases slightly strengthened with increasing temperature compared with those of P–Na. This suggests the promotion of doped carbonates to Na_4SiO_4 in CO_2 capture.

Decarbonization: When the temperature rose to 850 °C, the gas flow was changed to 100% N_2. In Figure 2d, Na_2CO_3 and Na_2SiO_3 phases were always present from 850 to 50 °C, and the weak intensity of Na_4SiO_4 was detected. The desorption did not proceed completely because the time spent in desorption was not long enough, and the temperature decreased gradually. In Figure 2e,f, the intensities of the Na_2SiO_3 phases weakened rapidly, and the Na_4SiO_4 phase appeared with higher intensity than that of the P–Na. When the temperature dropped from 850 to 765 °C, the Na_2CO_3 phases could be found in Figure 2e,f. This was because the product Na_2CO_3 and the mixed carbonates formed a melt at higher temperatures. As the temperature continued to decrease, the Na_2SiO_3 phase was observed. This indicates that the promotion of doped carbonates in desorption was less pronounced than in adsorption.

In situ XRD characterization of the carbonate-doped Na_4SiO_4 indicated that alkali carbonates could speed up the reaction of Na_4SiO_4 and CO_2 to form Na_2CO_3 and Na_2SiO_3, and no other impurity phases appeared. This is quite different from the results proposed by other studies on CO_2 capture by Na_2SiO_3 to produce SiO_2 [28]. During the CO_2 uptake process, the doped alkali carbonates worked as a facilitator during CO_2 uptake and did not change the reaction direction from the reactant Na_4SiO_4 to the final products Na_2SiO_3 and Na_2CO_3. For decarbonization, the weak peak intensity of the Na_4SiO_4 phase below 800 °C indicated the small contribution of carbonates to regenerating the Na_4SiO_4.

3.3. In Situ Raman

To investigate the structural transformation during CO_2 uptake by carbonate–doped Na_4SiO_4, samples of 10(LiNa)90Na and 10(LiNaK)90Na were used as representatives characterized by in situ high–temperature Raman. Figure 4 shows the in situ Raman results measured from room temperature to 800 °C in an atmosphere containing 80 vol% CO_2 in the wavenumber range of 500 to 1700 cm^{-1}. These Raman–type peaks contained two fundamental vibrational modes: v_1–symmetric stretching vibrations and v_3–asymmetric stretching vibrations, associated with CO_3^{2-}, $C_2O_5^{2-}$, SiO_3^{2-} and SiO_4^{4-} ions [34,39–42]. At ambient temperature, it was detected that typic peaks at 823 cm^{-1} related to the v_1 mode of Si–O in Na_4SiO_4 [41], and 1078 cm^{-1} were related to the v_1 mode of C–O in alkali carbonates [34]. When the temperature was above 100 °C, the peak of v_3 mode at 609 cm^{-1} and v_1 mode at 962 cm^{-1} of Si–O in Na_2SiO_3 [39,40,42] appeared, and the intensities strengthed gradually. Additionally, the peak intensity of v_1 mode at 1078 cm^{-1} related to C–O also exhibited a trend of gradual enhancement due to the product, Na_2CO_3. Correspondingly, the peak intensity of v_1 at 823 cm^{-1} related to Na_4SiO_4 showed a weakening trend. The peak at 1580 cm^{-1}, related to the v_1 mode of the specie $C_2O_5^{2-}$, was detected from 150 °C. These results indicate that the added alkali carbonates can exhibit significant promotion from 100 °C. Additionally, at temperatures below 300 °C, no melt

was present in the mixtures. This suggests that the pyrocarbonates can be emerged from solid carbonates and replace CO_2 to react with Na_4SiO_4, expressed as Equation (3).

$$C_2O_5^{2-} + Na_4SiO_4 = Na_2SiO_3 + Na_2CO_3 + CO_3^{2-} \quad (3)$$

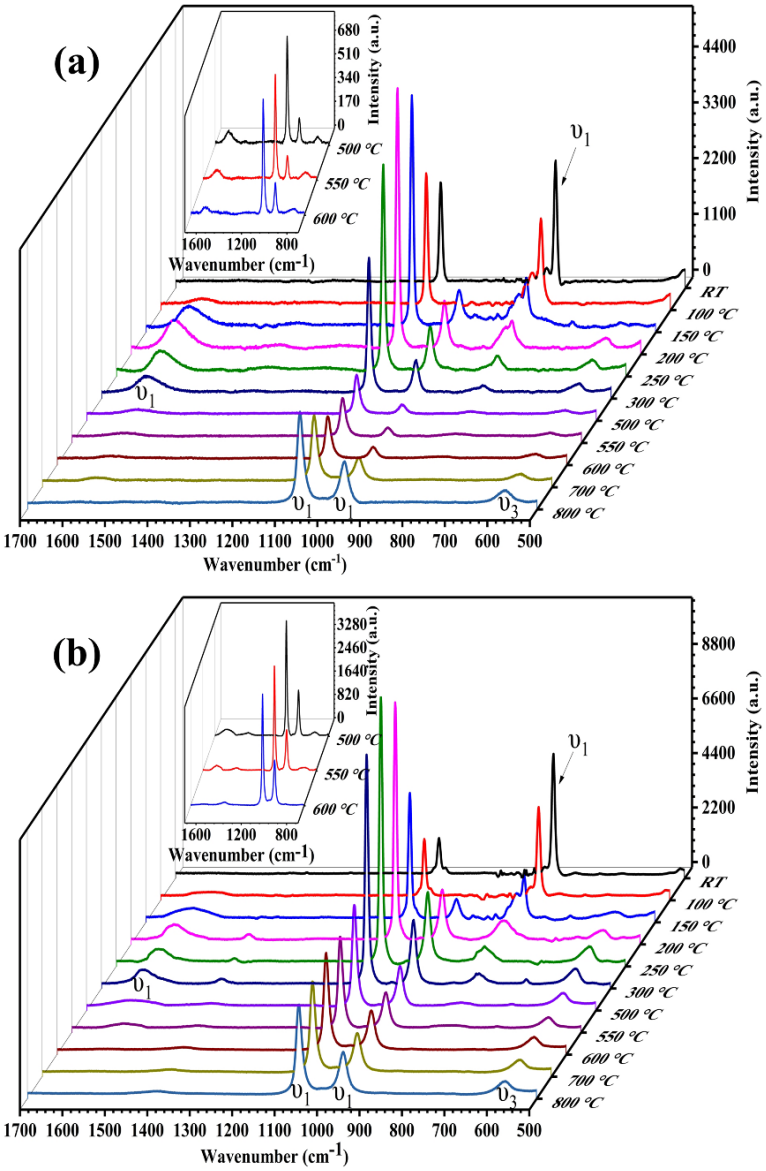

Figure 4. In situ Raman spectra of (**a**) 10(LiNa)90Na and (**b**) 10(LiNaK)90Na in the 80% CO_2 –20% N_2 atmosphere.

When the temperature rose above 500 °C, the carbonate melt was formed. The intensities of v_1 mode at 609 cm^{-1} and v_3 mode at 962 cm^{-1} related to the Si–O in Na_2SiO_3 maintained an upward trend when the temperature increased. Meanwhile, the intensity of v_1 at 1078 cm^{-1} assigned to CO_3^{2-} also showed a tendency to increase. The typical peaks of $C_2O_5^{2-}$ at 1580 cm^{-1} and Na_4SiO_4 at 823 cm^{-1} could also be found in the magnified view. The intensity of v_1 mode associated with Na_4SiO_4 at 823 cm^{-1} decreased significantly with increasing temperature, and this typic peak disappeared when it was higher than 600 °C. This revealed that the facilitating effect of alkali carbonate was manifested by the provision of pyrocarbonate and the formation of melt at higher than 500 °C, accelerating CO_2 transport and improving the CO_2 uptake performance.

3.4. Isothermal Analyses and Kinetic Evaluation

Dynamic thermal analyses of Na_4SiO_4 mixed with different amounts of alkali carbonates were performed from amient temperature to 900 °C in the 80% CO_2 –20% N_2 atmosphere, and the results were shown in Figures S1–S4. CO_2 uptake can be roughly divided into two temperature ranges, above and below 400 °C, corresponding to carbonate mixtures in solids and melts. Isothermal adsorption was performed in two temperature ranges, 200–300 °C and 500–600 °C, to clarify the facilitation of alkali carbonates in different phase states.

To explore the positive influence of solid carbonates in different quantities on the CO_2 sorption capacity of Na_4SiO_4, isothermal experiments were conducted at 200–300 °C for 120 min under an atmosphere containing 80% CO_2, and the results are shown in Figure 5a–c. The weight gain of all samples at different temperatures and the conversion of Na_4SiO_4 contained therein were listed in Table S1. The sorption capacity of all samples increased with increasing temperature. It was determined that the rate and adsorption capacity of CO_2 capture by Na_4SiO_4 were significantly enhanced at different temperatures due to the mixed alkali carbonates. At the same addition ratio, the improvement of Li_2CO_3–Na_2CO_3 seemed to be relatively close to that of Li_2CO_3–Na_2CO_3–K_2CO_3, and samples containing Li_2CO_3–Na_2CO_3 exhibited slightly better chemisorption. Among sorbents, 10(LiNa)90Na had the best CO_2 capture performance at 200–300 °C. The weight gain of 10(LiNa)90Na after sorption at 300 °C for 120 min was 13.3%, corresponding to $\chi_{Na_4SiO_4}$ = 58.6%. Under the same conditions, the weight gain of sample P–Na was 7.9%, corresponding to $\chi_{Na_4SiO_4}$ = 33.1%. However, the performance became worse when the carbonate content was doubled to 20 mol%.

To compare the contribution of molten carbonates and pyrocarbonates to the CO_2 sorption capacity of Na_4SiO_4, isothermal experiments were conducted at 500–600 °C for 120 min, and the results are shown in Figure 5d–f. In this temperature range, there was little difference in the promotion effect of binary and ternary carbonates. Overall, 5 mol% and 10 mol% of carbonates seemed to perform a similar promotion. At 500–600 °C, 10(LiNa)90Na showed the best CO_2 uptake performance among sorbents. The weight gain of 10(LiNa)90Na after sorption at 600 °C for 120 min was 16.7 %, corresponding to $\chi_{Na_4SiO_4}$ = 74.9%. Under the same conditions, the weight gain of sample P–Na was 13.8 %, corresponding to $\chi_{Na_4SiO_4}$ = 57.7%. However, the CO_2 uptake performance became poor when the carbonate content was doubled to 20 mol%. It is suggested that the appropriate amount of alkali carbonate addition is critical to enhancing the CO_2 capture performance of Na_4SiO_4. Therefore, when the molar ratios of alkali carbonates in the samples are the same, the samples containing Li_2CO_3–Na_2CO_3 or Li_2CO_3–Na_2CO_3–K_2CO_3 show similar CO_2 uptake performance at the same experimental temperatures.

Taking P–Na, 10(LiNa)90Na, and 20(LiNa)80Na as representatives, the CO_2 sorption results of the samples were simulated by a double exponential model [14,27,43] expressed as Equation (4), in which y is the weight gain of CO_2 sorbents, t is the CO_2 uptake time, A_1, A_2, and A_3 are the pre-exponential factors, and k_1 and k_2 are the exponential constants for chemisorption and bulk diffusion, respectively. As shown in Tables 1 and 2, the value of the chemisorption rate (k_1) is an order of magnitude greater than that of the bulk diffusion rate (k_2) for all samples. The values of k_1 and k_2 for all samples at 500–600 °C were greater than those of samples at 200–300 °C. This indicates that the carbonates were more effective when they were in melt compared to solid form. The values of k_1 and k_2 for 10(LiNa)90Na were also greater than those of P–Na and 20(LiNa)80Na, which means that 10 mol% was a more appropriate additive amount at different temperatures.

$$y = A_1 \cdot \exp(-k_1 \cdot t) + A_2 \cdot \exp(-k_2 \cdot t) + A_3 \quad (4)$$

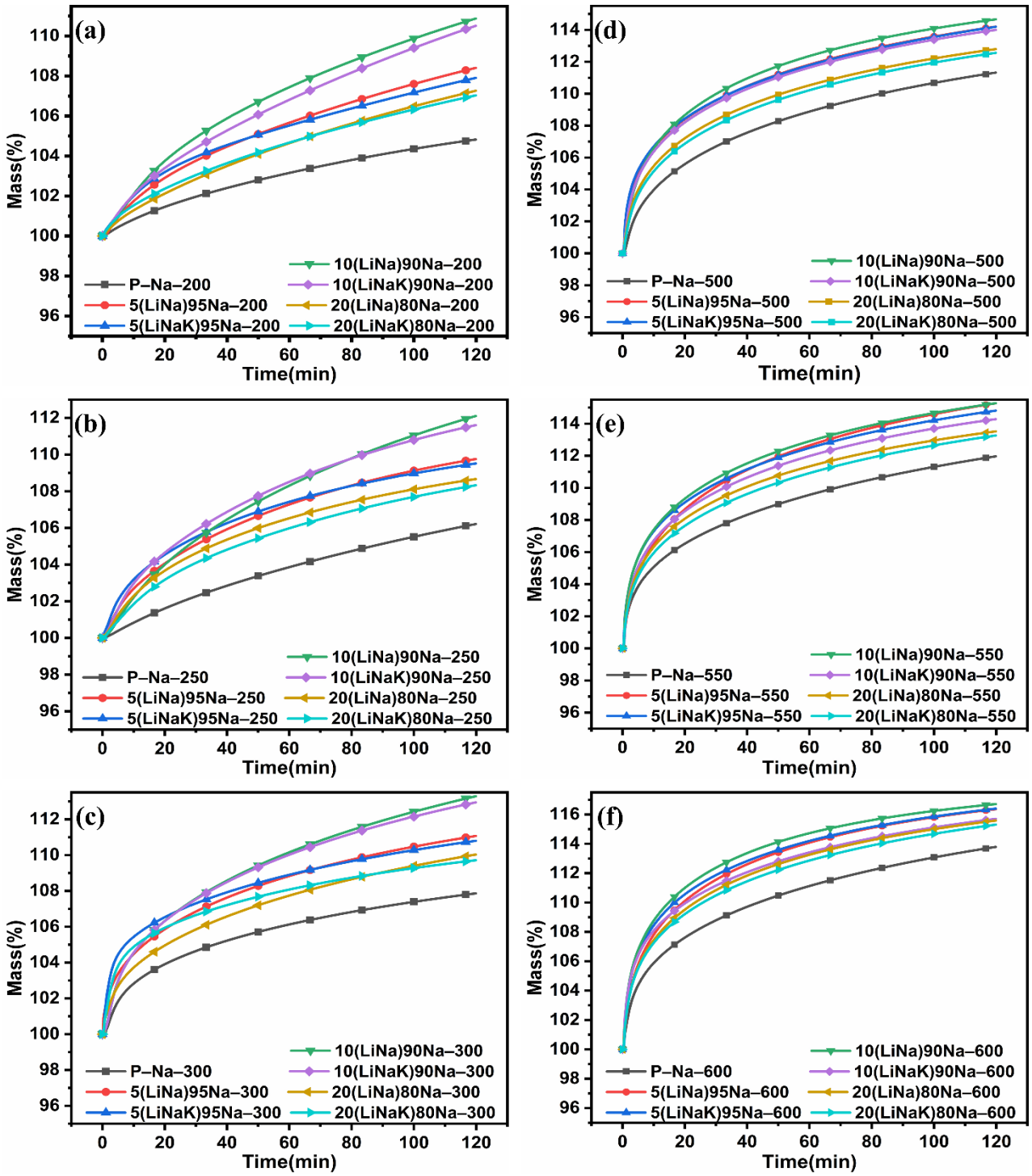

Figure 5. Isothermal analyses of Na_4SiO_4 with different carbonates at (**a**–**c**) 200–300 °C and (**d**–**f**) 500–600 °C in the atmosphere containing 80% CO_2.

Table 1. Kinetic parameters of P–Na, 10(LiNa)90Na, and 20(LiNa)80Na at 200–300 °C.

Sample	T (°C)	k_1 (s^{-1})	k_2 (s^{-1})	R^2
P–Na	200	1.21×10^{-3}	1.21×10^{-4}	0.999
	250	1.93×10^{-3}	1.56×10^{-4}	0.999
	300	2.89×10^{-3}	2.10×10^{-4}	0.999
10(LiNa)90Na	200	1.97×10^{-3}	2.21×10^{-4}	0.999
	250	2.73×10^{-3}	2.66×10^{-4}	0.999
	300	3.81×10^{-3}	3.10×10^{-4}	0.999
20(LiNa)80Na	200	1.57×10^{-3}	1.58×10^{-4}	0.999
	250	2.24×10^{-3}	1.96×10^{-4}	0.999
	300	3.25×10^{-3}	2.45×10^{-4}	0.999

Table 2. Kinetic parameters of P–Na, 10(LiNa)90Na, and 20(LiNa)80Na at 500–600 °C.

Sample	T (°C)	k_1 (s^{-1})	k_2 (s^{-1})	R^2
P–Na	500	2.91×10^{-3}	2.01×10^{-4}	0.999
	550	3.46×10^{-3}	2.29×10^{-4}	0.999
	600	4.23×10^{-3}	2.63×10^{-4}	0.999
10(LiNa)90Na	500	4.56×10^{-3}	2.96×10^{-4}	0.999
	550	5.13×10^{-3}	3.21×10^{-4}	0.999
	600	5.71×10^{-3}	3.47×10^{-4}	0.999
20(LiNa)80Na	500	3.34×10^{-3}	2.27×10^{-4}	0.999
	550	3.88×10^{-3}	2.51×10^{-4}	0.999
	600	4.49×10^{-3}	2.76×10^{-4}	0.999

To provide further discussion on the temperature dependence of alkali carbonates at 200–300 °C on CO_2 capture by Na_4SiO_4, the activation energies of chemisorption and bulk diffusion for P–Na, 10(LiNa)90Na, and 20(LiNa)80Na were simulated according to the Eyring's model [14] expressed as Equation (5), in which k denotes the reaction rate constant, i.e., k_1 and k_2 above. t denotes the absolute temperature in units of K^{-1}. R is the gas constant 8.314 $J{\cdot}mol^{-1}{\cdot}K^{-1}$. k_B is the Boltzmann constant 1.380649×10^{-23} $J{\cdot}K^{-1}$. h is the Planck constant $6.62607015 \times 10^{-34}$ J·s. ΔH^{++} and ΔS^{++} represent the activation enthalpy and activation entropy, respectively, which can be fitted to obtain

$$\ln(k/T) = -\Delta H^{++}/(\mathrm{RT}) + ln(k_B/h) + \Delta S^{++}/\mathrm{R}. \quad (5)$$

Accordingly, the fitted functional relationship of k and T is shown in Figure 6a. The mixed alkali carbonates lead to a decline in the activation energy of chemisorption and diffusion for CO_2 capture of Na_4SiO_4. In the case of chemisorption, the fitted activation energies were 15.30, 10.50, and 12.03 $kJ{\cdot}mol^{-1}$ for P–Na, 10(LiNa)90Na, and 20(LiNa)80Na, respectively, which means that the carbonates can diminish the temperature dependence of chemisorption of Na_4SiO_4. Combined with in situ Raman characterization, it can be inferred that the doped carbonate opens up new chemical reaction pathways, as expressed in Equation (3), which greatly accelerates the CO_2 uptake reaction and diminishes the activation energy of chemisorption. In terms of the bulk diffusion, the activation energy of P–Na was 8.07 $kJ{\cdot}mol^{-1}$, and it dropped to 3.34 and 5.41 $kJ{\cdot}mol^{-1}$ for 10(LiNa)90Na and 20(LiNa)80Na, respectively. The significant reduction in activation energy was attributed to the formation of pyrocarbonates, which reacted with Na_4SiO_4, followed by the release of CO_3^{2-} and its recombination with CO_2. The oxo-Grothuss mechanism could improve the CO_2 uptake kinetics of Na_4SiO_4 [24]. However, more alkali carbonate content in the sorbents did not necessarily lead to better chemisorption. For 20(LiNa)80Na, the diffusion process required more activation energy than that of 10(LiNa)90Na, which indicates that too much alkali carbonates covering the sorbent surface will block the diffusion of CO_2.

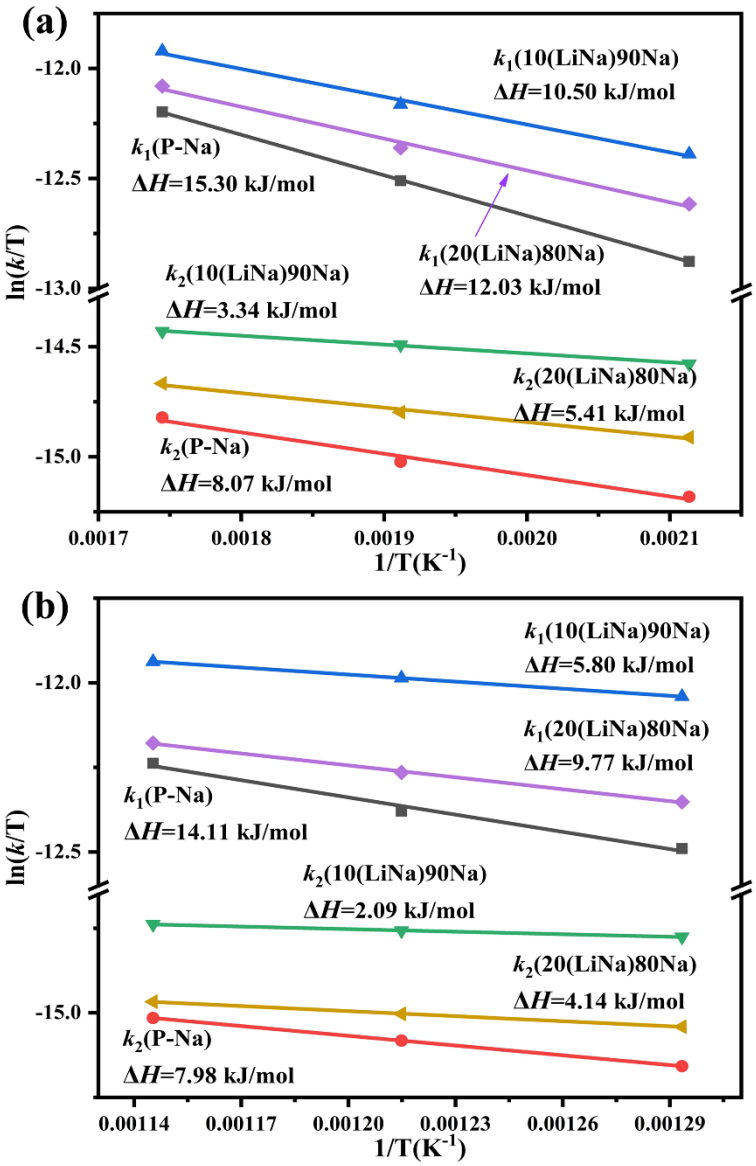

Figure 6. Eyring type profiles of k_1 and k_2 for different samples at (**a**) 200–300 °C and (**b**) 500–600 °C.

The activation energies of chemisorption and diffusion for P–Na, 10(LiNa)90Na, and 20(LiNa)80Na at 500–600 °C were evaluated by Eyring's model. As shown in Figure 6b, the addition of alkali carbonates contributed to a remarkable decrement in the activation enthalpy for chemisorption and bulk diffusion of CO_2 capture by Na_4SiO_4. The ΔH^{++} values of chemisorption calculated were 14.11, 5.80, and 9.77 kJ·mol^{-1} for P–Na, 10(LiNa)90Na, and 20(LiNa)80Na, respectively, which means that mixed alkaline carbonates result in the reduced temperature dependence of chemisorption. In the case of the diffusion process, the ΔH^{++} of P–Na was 7.98 kJ·mol^{-1}, and the values of 10(LiNa)90Na and 20(LiNa)80Na dropped to 2.09 and 4.14 kJ·mol^{-1}, respectively. In contrast, the activation energies of both chemisorption and bulk diffusion were found to be further reduced at 500–600 °C than at 200–300 °C, especially for bulk diffusion. Combined with in situ Raman characterization, it can be concluded that at 500–600 °C, pyrocarbonate and molten carbonates make joint contributions to the CO_2 uptake of Na_4SiO_4. The pyrocarbonate breaks up a new CO_2 uptake pathway, and the molten carbonate reduces the resistance to CO_2 diffusion. Therefore, polycarbonates can significantly improve the kinetics of CO_2 capture by Na_4SiO_4. However, when the content of alkali carbonates was added to 20 mol%, the diffusion process required more activation energy than that of 10(LiNa)90Na, which was attributed to excessive carbonate melts, hindering CO_2 diffusion to Na_4SiO_4.

SEM images of P–Na and 10(LiNa)90Na after isothermal experiments at 300 °C and 600 °C are shown in Figure 7. For P–Na, after two hours of isothermal analysis at 300 °C, the overall morphology did not change much, and the surface showed dense particles in Figure 7a. As shown in Figure 7b, when the temperature was up to 600 °C and isothermal analysis was carried out for two hours, the large particles were refined into small particles after the reaction. However, in individual areas, only some traces of surface reaction could be observed. For 10(LiNa)90Na, after two hours of isothermal chemisorption at 300 °C, there was a distribution of fine particles on the surface of large particles, and some areas of unreacted material were exposed, as shown in Figure 7c. In Figure 7d, the reaction product of 10(LiNa)90Na was distributed in small particles and had a certain number of small sparse pores distributed on the surface. Alkali carbonates changed the morphology of Na_4SiO_4, refining the particles and forming a porous structure, thus increasing the reactivity of Na_4SiO_4.

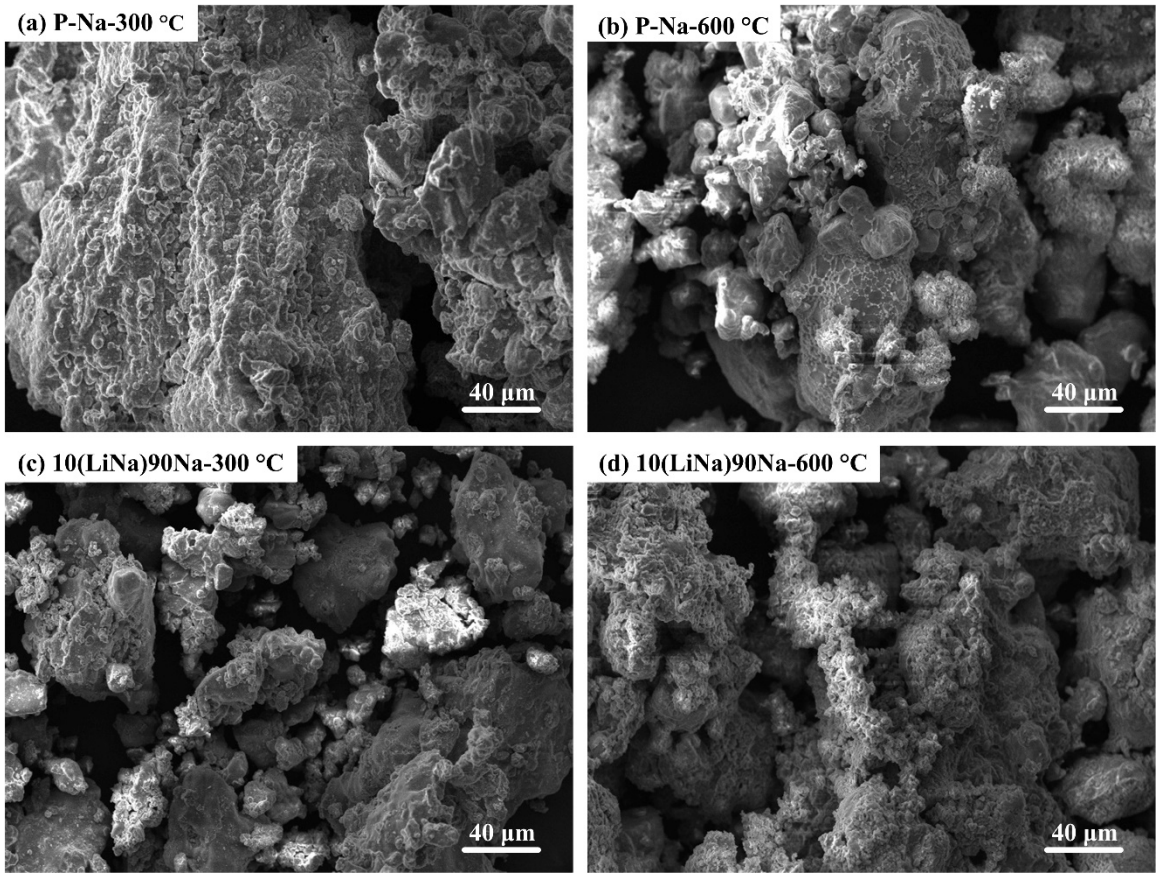

Figure 7. SEM images of P–Na and 10(LiNa)90Na after isothermal sorption at 300 °C and 600 °C.

The CO_2 capture capacities of Na_4SiO_4 phasically doped with different alkali carbonates under different experimental conditions were compared, as shown in Table 3. The contribution of single alkali carbonates to CO_2 uptake varied by species and proportion for different Na_4SiO_4-based sorbents. Larger proportions of alkali carbonates in sorbents did not imply better facilitation. In this study, alkali carbonates were employed to accelerate CO_2 capture and were found to significantly improve the CO_2 uptake performance of Na_4SiO_4, especially at lower temperatures.

Table 3. Weight gain of Na_4SiO_4-based sorbents under different experimental conditions.

Sample	Dopant	Sorption Conditions	Weight Gain, %	Reference
Na_2CO_3-Fly ash	-	Isothermally, 700 °C, 100% CO_2, 120 min	9.8	A. Sanna [27]
Na_2CO_3-Fly ash	5 mol% Li_2CO_3	Isothermally, 700 °C, 100% CO_2, 120 min	10.2	A. Sanna [27]
Na_2CO_3-Fly ash	10 mol% Li_2CO_3	Isothermally, 700 °C,100% CO_2, 120 min	11.4	A. Sanna [27]
Na_2CO_3-Fly ash	10 mol% K_2CO_3	Isothermally, 700 °C,100% CO_2, 120 min	9.9	A. Sanna [27]
Na_4SiO_4	33.3 wt% Li_2CO_3	Dynamic thermally, 50–1000 °C, 80% CO_2	14.9	Liu [24]
Na_4SiO_4	33.3 wt% Na_2CO_3	Dynamic thermally, 50–1000 °C, 80% CO_2	7.7	Liu [24]
Na_4SiO_4	33.3 wt% K_2CO_3	Dynamic thermally, 50–1000 °C, 80% CO_2	10.8	Liu [24]
Na_4SiO_4	33.3 mol% Na_2CO_3	Isothermally, 550 °C, Air, 190 min	3.2	Wang [25]
Na_4SiO_4	-	Isothermally, 300 °C, 80% CO_2, 120 min	7.9	This work
Na_4SiO_4	-	Isothermally, 600 °C, 80% CO_2, 120 min	13.8	This work
Na_4SiO_4	10 mol% (Li_2CO_3-Na_2CO_3)	Isothermally, 300 °C, 80% CO_2, 120 min	13.3	This work
Na_4SiO_4	10 mol% (Li_2CO_3-Na_2CO_3)	Isothermally, 600 °C, 80% CO_2, 120 min	16.7	This work

3.5. Cyclic Stability

Multiple absorption–desorption cycles were conducted to study the influence of doped carbonate on the long-term stability of CO_2 capture, and the results are shown in Figure 8. 10(LiNa)90Na was selected for cyclic experiments because of its better performance in isothermal analyses. As shown in Figure 8a, for P–Na, the first adsorption capacity was close to 50% of the theoretical value, but the desorption was 26% of the theoretical value. In the following 19 cycles, adsorption and desorption tended to be stable, reaching 30% of the theoretical conversion. In Figure 8b, for 10(LiNa)90Na, the capacity reached 60% of its theoretical value in the first adsorption, but desorption was not carried out completely. In the following 19 cycles, the capacity of adsorption and desorption increased gradually. The conversion finally reached 52% of the theoretical value. In general, alkali carbonates contributed greatly to the durability of CO_2 capture by Na_4SiO_4. It is suggested that molten carbonates can disperse the reaction products of Na_4SiO_4 and CO_2, reducing the aggregation of products. The gradual improvement of conversion is due to the redistribution of products and regeneration products in multiple cycles so that unreacted Na_4SiO_4 can contact and react with CO_2.

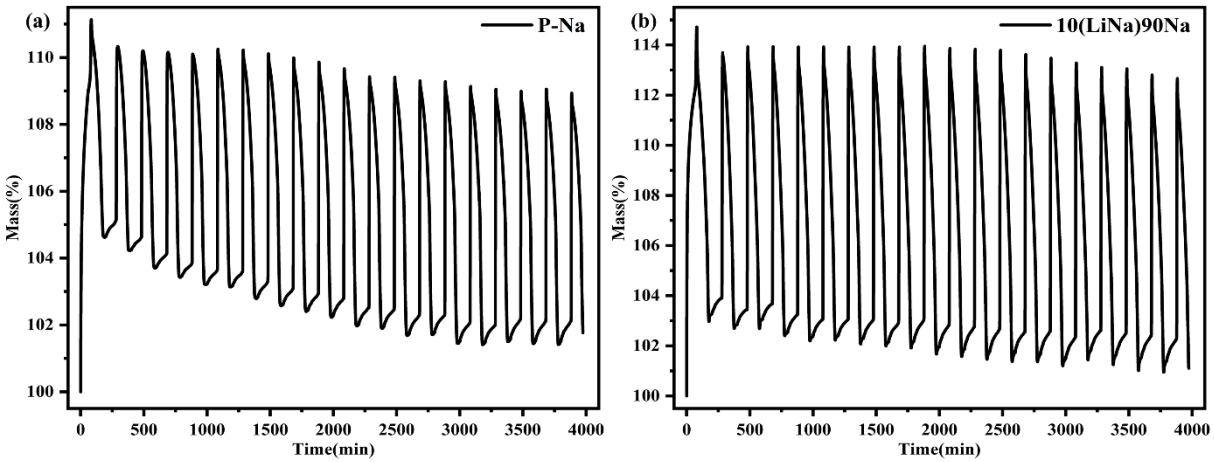

Figure 8. Cyclic stability of (**a**) P–Na and (**b**) 10(LiNa)90Na.

4. Conclusions

In this study, it was confirmed that the CO_2 uptake performance of Na_4SiO_4 can be effectively enhanced when mixed with Li_2CO_3–Na_2CO_3 or Li_2CO_3–Na_2CO_3–K_2CO_3. Compared with P–Na, alkali carbonate-doped Na_4SiO_4 achieved CO_2 capture from 100 °C. This is due to the fact that the alkali carbonates reacted with CO_2 at different temperatures

to form pyrocarbonates, $C_2O_5^{2-}$, which in turn reacted with Na_4SiO_4 to form Na_2SiO_3, as shown in Figure 9. When the temperature is higher than the eutectic point of alkali carbonates, the molten alkali carbonates become a carrier to accelerate CO_2 diffusion. When the temperature is above 800 °C, the spent Na_4SiO_4 will be regenerated due to the reaction between the products of Na_2SiO_3 and Na_2CO_3, whereafter CO_2 is released. In the CO_2 desorption, the molten alkali carbonates seem to provide liquid channels for CO_2 diffusion through the solid product layers.

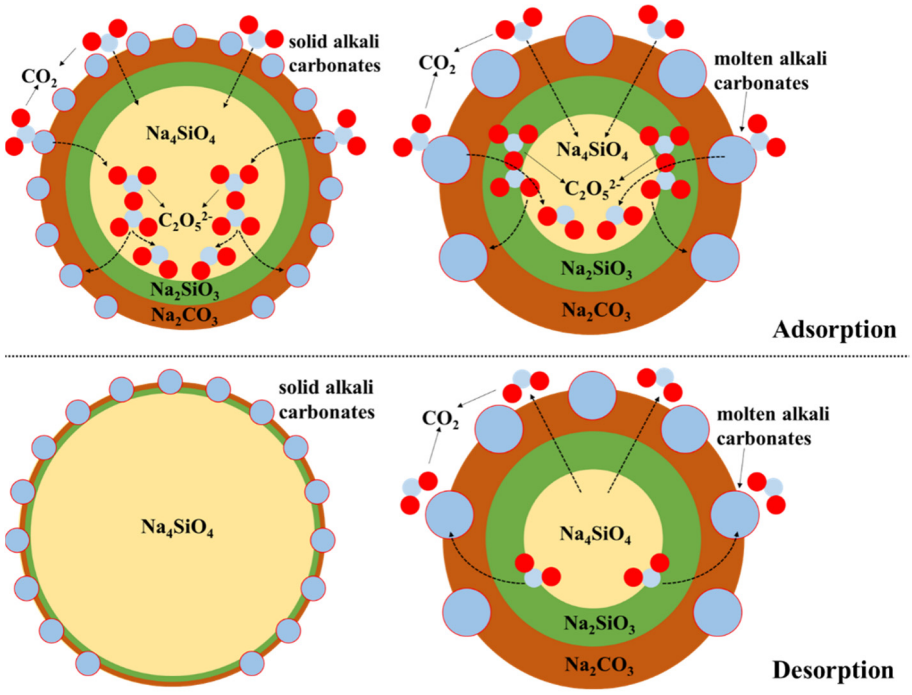

Figure 9. Schematic illustration of the CO_2 sorption and desorption pathway for the Na_4SiO_4 mixed alkali carbonates.

When the proportion of alkali carbonates in the sorbents was the same, there was little difference in the promotion between binary and ternary alkali carbonates. The CO_2 uptake capacity of carbonate-doped Na_4SiO_4 increased dramatically as the proportion of carbonates was increased from 5 to 10 mol%. Overall, 10 mol% of Li_2CO_3–Na_2CO_3 was found to be the optimum addition for CO_2 capture of Na_4SiO_4 and exhibited the best CO_2 uptake capacity at different temperatures. At 200–300 °C, the activation energy values of the chemisorption and the bulk diffusion were 12.03 kJ·mol^{-1} and 3.34 kJ·mol^{-1}, respectively, corresponding to 15.30 kJ·mol^{-1} and 8.07 kJ·mol^{-1} for pristine Na_4SiO_4. This was attributed to the fact that alkali carbonates could bind CO_2 to produce pyrocarbonates, $C_2O_5^{2-}$. The alkali pyrocarbonates were formed at 100 °C and reacted with Na_4SiO_4, followed by the release of CO_3^{2-} and its recombination with CO_2. The Grothuss-like mechanism improved the CO_2 uptake kinetics of Na_4SiO_4 when doped carbonates were present in the solid state. At 500–600 °C, the enhancement of carbonates was more pronounced, as both pyrocarbonates and melts worked simultaneously. The activation energy values of chemisorption and bulk diffusion for 10(LiNa)90Na were 7.98 kJ·mol^{-1} and 2.09 kJ·mol^{-1}, respectively, which were lower than those of 14.11 kJ·mol^{-1} and 5.80 kJ·mol^{-1} for pristine Na_4SiO_4. In addition, alkali carbonates significantly improved the cycle stability of CO_2 captured by Na_4SiO_4. After 20 cycles, the conversion of Na_4SiO_4 mixed with 10 mol% Li_2CO_3–Na_2CO_3 exceeded 52% of the theoretical value, which was much higher than 26% for the pristine Na_4SiO_4.

In conclusion, the CO_2 capture performance of Na_4SiO_4 was improved by alkali carbonates in solid and melt states, which were both beneficial for the CO_2 uptake kinetics

of Na_4SiO_4. Future efforts will be focused on CO_2 desorption performance and cyclic stability to develop economical Na_4SiO_4-based CO_2 sorbents.

Supplementary Materials: The following supporting information can be downloaded at: https://www.mdpi.com/article/10.3390/separations9120428/s1, Figure S1: TG–DSC curves of P–Na at 50–900 °C with a heating rate of 10 °C·min^{-1} in the 80%CO_2–20%N_2 atmosphere; Dashed line: TG curves of Li_4SiO_4; Figure S2: TG–DSC curves of 5(LiNa)95Na (a) and 5(LiNaK)95Na (b) at 50–900 °C with a heating rate of 10 °C·min^{-1} in the 80%CO_2–20%N_2 atmosphere; Dashed line: TG curves of P–Na.; Figure S3: TG–DSC curves of 10(LiNa)90Na (a) and 10(LiNaK)90Na (b) at 50–900 °C with a heating rate of 10 °C·min^{-1} in the 80%CO_2–20%N_2 atmosphere; Dashed line: TG curves of P–Na.; Figure S4: TG–DSC curves of 20(LiNa)80Na (a) and 20(LiNaK)80Na (b) at 50–900 °C with a heating rate of 10 °C·min^{-1} in the 80%CO_2–20%N_2 atmosphere; Dashed line: TG curves of P–Na.; Table S1. Weight gain and conversion of different samples at different temperatures.

Author Contributions: Conceptualization, Q.X. and Z.W.; methodology, Z.W.; validation, C.S., H.C. and X.Z.; formal analysis, Z.W.; investigation, Z.W.; resources, Q.X. and X.L.; data curation, Z.W.; writing—original draft preparation, Z.W.; writing—review and editing, Z.W.; visualization, C.S.; supervision, X.L.; project administration, Q.X. and X.L.; funding acquisition, Q.X. and X.L. All authors have read and agreed to the published version of the manuscript. Authorship was limited to those who contributed substantially to the work reported.

Funding: This research was funded by the National Natural Science Foundation of China (No. 51574163) and the Science and Technology Commission of Shanghai Municipality (Grant No. 21DZ1208900).

Institutional Review Board Statement: Not applicable.

Informed Consent Statement: Not applicable.

Data Availability Statement: Not applicable.

Acknowledgments: This work was financially supported by the National Natural Science Foundation of China (No. 51574163) and the Science and Technology Commission of Shanghai Municipality (Grant No. 21DZ1208900). The authors would like to acknowledge everyone for their help a in equipment support, experimental guidance and theoretical analyses. Special thanks to Jinglin You, Xueguang Wang and Guangshi Li at Shanghai University for their great help in characterizations of Raman, SEM, and XRD.

Conflicts of Interest: The authors declare no conflict of interest.

References

1. Crippa, M.; Oreggioni, G.; Guizzardi, D.; Muntean, M.; Schaaf, E.; Lo Vullo, E.; Solazzo, E.; Monforti-Ferrario, F.; Olivier, J.G.; Vignati, E. *Fossil CO_2 and GHG Emissions of All World Countries*; Publication Office of the European Union: Luxembourg, 2017.
2. Robinson, S.A. Climate change adaptation in SIDS: A systematic review of the literature pre and post the IPCC Fifth Assessment Report. *Wiley Interdiscip. Rev. Clim. Change* **2020**, *11*, e653. [CrossRef]
3. Bui, M.; Adjiman, C.S.; Bardow, A.; Anthony, E.J.; Boston, A.; Brown, S.; Fennell, P.S.; Fuss, S.; Galindo, A.; Hackett, L.A. Carbon capture and storage (CCS): The way forward. *Energy Environ. Sci.* **2018**, *11*, 1062–1176. [CrossRef]
4. Selma, L.; Seigo, O.; Dohle, S.; Siegrist, M. Public perception of carbon capture and storage (CCS): A review. *Renew. Sustain. Energy Rev.* **2014**, *38*, 848–863.
5. Valverde, J.M. Ca-based synthetic materials with enhanced CO 2 capture efficiency. *J. Mater. Chem. A* **2013**, *1*, 447–468. [CrossRef]
6. Tomkute, V.; Solheim, A.; Olsen, E. CO_2 capture by CaO in molten CaF_2–$CaCl_2$: Optimization of the process and cyclability of CO_2 capture. *Energy Fuels* **2014**, *28*, 5345–5353. [CrossRef]
7. Nygård, H.S.; Tomkute, V.; Olsen, E. Kinetics of CO_2 absorption by calcium looping in molten halide salts. *Energy Procedia* **2017**, *114*, 250–258. [CrossRef]
8. Jo, S.-I.; An, Y.-I.; Kim, K.-Y.; Choi, S.-Y.; Kwak, J.-S.; Oh, K.-R.; Kwon, Y.-U. Mechanisms of absorption and desorption of CO_2 by molten $NaNO_3$-promoted MgO. *Phys. Chem. Chem. Phys.* **2017**, *19*, 6224–6232. [CrossRef]
9. Wang, L.; Zhou, Z.; Hu, Y.; Cheng, Z.; Fang, X. Nanosheet MgO-based CO_2 sorbent promoted by mixed-alkali-metal nitrate and carbonate: Performance and mechanism. *Ind. Eng. Chem. Res.* **2017**, *56*, 5802–5812. [CrossRef]
10. Pfeiffer, H. Advances on alkaline ceramics as possible CO_2 captors. In *Advances in CO_2 Conversion and Utilization*; ACS Publications: Washington, DC, USA, 2010; pp. 233–253.

11. Peltzer, D.; Mùnera, J.; Cornaglia, L.; Strumendo, M. Characterization of potassium doped Li_2ZrO_3 based CO_2 sorbents: Stability properties and CO_2 desorption kinetics. *Chem. Eng. J.* **2018**, *336*, 1–11. [CrossRef]
12. Olivares-Marín, M.; Castro-Díaz, M.; Drage, T.C.; Maroto-Valer, M.M. Use of small-amplitude oscillatory shear rheometry to study the flow properties of pure and potassium-doped Li2ZrO3 sorbents during the sorption of CO_2 at high temperatures. *Sep. Purif. Technol.* **2010**, *73*, 415–420. [CrossRef]
13. Munro, S.; Åhlén, M.; Cheung, O.; Sanna, A. Tuning Na_2ZrO_3 for fast and stable CO_2 adsorption by solid state synthesis. *Chem. Eng. J.* **2020**, *388*, 124284. [CrossRef]
14. Mendoza-Nieto, J.A.; Martínez-Hernández, H.; Pfeiffer, H.; Gómez-García, J.F. A new kinetic model for CO_2 capture on sodium zirconate (Na_2ZrO_3): An analysis under different flow rates. *J. CO2 Util.* **2022**, *56*, 101862. [CrossRef]
15. Halliday, C.; Ozbek, N.; Hatton, T.A. Understanding Material Compatibility in CO_2 Capture Systems Using Molten Alkali Metal Borates. *ACS Appl. Mater. Interfaces* **2020**, *12*, 51468–51477. [CrossRef]
16. Halliday, C.; Harada, T.; Hatton, T.A. Bench-Scale Demonstration of Molten Alkali Metal Borates for High-Temperature CO_2 Capture. *Ind. Eng. Chem. Res.* **2020**, *59*, 8937–8945. [CrossRef]
17. Kibar, M.E.; Akın, A.N. A novel process for CO_2 capture by using sodium metaborate. Part I: Effects of calcination. *Environ. Sci. Pollut. Res.* **2018**, *25*, 3446–3457. [CrossRef]
18. Kibar, M.E.; Akin, A.N. A Novel Process for CO_2 Capture by Using Sodium Metaborate, Part II: Carbonation Reaction and Kinetic Studies. *Int. J. Chem. Kinet.* **2017**, *49*, 119–129. [CrossRef]
19. Bernabé-Pablo, E.; Duan, Y.; Pfeiffer, H. Developing new alkaline ceramics as possible CO2 chemisorbents at high temperatures: The lithium and sodium yttriates ($LiYO_2$ and $NaYO_2$) cases. *Chem. Eng. J.* **2020**, *396*, 125277. [CrossRef]
20. Cruz, D.; Bulbulian, S.; Lima, E.; Pfeiffer, H. Kinetic analysis of the thermal stability of lithium silicates (Li_4SiO_4 and Li_2SiO_3). *J. Solid State Chem.* **2006**, *179*, 909–916. [CrossRef]
21. Seggiani, M.; Puccini, M.; Vitolo, S. Alkali promoted lithium orthosilicate for CO2 capture at high temperature and low concentration. *Int. J. Greenh. Gas Control.* **2013**, *17*, 25–31. [CrossRef]
22. Seggiani, M.; Stefanelli, E.; Puccini, M.; Vitolo, S. CO_2 sorption/desorption performance study on K_2CO_3-doped Li_4SiO_4-based pellets. *Chem. Eng. J.* **2018**, *339*, 51–60. [CrossRef]
23. Sanna, A.; Ramli, I.; Maroto-Valer, M.M. Development of sodium/lithium/fly ash sorbents for high temperature post-combustion CO_2 capture. *Appl. Energy* **2015**, *156*, 197–206. [CrossRef]
24. Liu, J.; Wang, Z.; Wang, Z.; Song, J.; Li, G.; Xu, Q.; You, J.; Cheng, H.; Lu, X. Alkali carbonates promote CO_2 capture by sodium orthosilicate. *Phys. Chem. Chem. Phys.* **2019**, *21*, 13135–13143. [CrossRef]
25. Wang, Z.R.; Liu, W.H.; Tang, Z.F.; Xu, Q. In situ Raman and XRD study of CO_2 sorption and desorption in air by a Na_4SiO_4-Na_2CO_3 hybrid sorbent. *Phys. Chem. Chem. Phys.* **2020**, *22*, 27263–27271. [CrossRef]
26. Sanna, A.; Ramli, I.; Maroto-Valer, M.M. Novel Na-silicates CO_2 sorbents from fly ash. *Energy Procedia* **2014**, *63*, 739–744. [CrossRef]
27. Sanna, A.; Maroto-Valer, M.M. CO_2 capture at high temperature using fly ash-derived sodium silicates. *Ind. Eng. Chem. Res.* **2016**, *55*, 4080–4088. [CrossRef]
28. Rodríguez, M.T.; Pfeiffer, H. Sodium metasilicate (Na_2SiO_3): A thermo-kinetic analysis of its CO_2 chemical sorption. *Thermochim. Acta* **2008**, *473*, 92–95. [CrossRef]
29. Rodríguez-Mosqueda, R.; Pfeiffer, H. High CO_2 capture in sodium metasilicate (Na_2SiO_3) at low temperatures (30–60 °C) through the CO_2–H_2O chemisorption process. *J. Phys. Chem. C* **2013**, *117*, 13452–13461. [CrossRef]
30. Kwak, J.-S.; Oh, K.-R.; Kim, K.-Y.; Lee, J.-M.; Kwon, Y.-U. CO_2 absorption and desorption characteristics of MgO-based absorbent promoted by triple eutectic alkali carbonate. *Phys. Chem. Chem. Phys.* **2019**, *21*, 20805–20813. [CrossRef]
31. Huang, L.; Zhang, Y.; Gao, W.; Harada, T.; Qin, Q.; Zheng, Q.; Hatton, T.A.; Wang, Q. Alkali carbonate molten salt coated calcium oxide with highly improved carbon dioxide capture capacity. *Energy Technol.* **2017**, *5*, 1328–1336. [CrossRef]
32. Martinez-dlCruz, L.; Pfeiffer, H. Effect of Oxygen Addition on the Thermokinetic Properties of CO_2 Chemisorption on Li_2ZrO_3. *Ind. Eng. Chem. Res.* **2010**, *49*, 9038–9042. [CrossRef]
33. Wang, Z.; Xu, Q.; Peng, K.; Wang, Z.; Zou, X.; Cheng, H.; Lu, X. Elucidating the promotion of Na_2CO_3 in CO_2 capture by Li_4SiO_4. *Phys. Chem. Chem. Phys.* **2021**, *23*, 26696–26708. [CrossRef]
34. Zhang, L.; Huang, X.; Qin, C.; Brinkman, K.; Gong, Y.; Wang, S.; Huang, K. First spectroscopic identification of pyrocarbonate for high CO 2 flux membranes containing highly interconnected three dimensional ionic channels. *Phys. Chem. Chem. Phys.* **2013**, *15*, 13147–13152. [CrossRef]
35. Corradini, D.; Coudert, F.-X.; Vuilleumier, R. Carbon dioxide transport in molten calcium carbonate occurs through an oxo-Grotthuss mechanism via a pyrocarbonate anion. *Nat. Chem.* **2016**, *8*, 454–460. [CrossRef]
36. Jo, H.G.; Yoon, H.J.; Lee, C.H.; Lee, K.B. Citrate sol–gel method for the preparation of sodium zirconate for high-temperature CO_2 sorption. *Ind. Eng. Chem. Res.* **2016**, *55*, 3833–3839. [CrossRef]
37. Martínez-dlCruz, L.; Pfeiffer, H. Cyclic CO_2 chemisorption–desorption behavior of Na_2ZrO_3: Structural, microstructural and kinetic variations produced as a function of temperature. *J. Solid State Chem.* **2013**, *204*, 298–304. [CrossRef]
38. Habibi-Khorassani, S.M.; Maghsoodlou, M.T.; Shahraki, M.; Talaiefar, S.; Kazemian, M.A.; Aboonajmi, J. Full kinetics and a mechanistic investigation of three-component reaction catalyzed by sodium acetate leading to 3, 4-dihydropyrano [c] chromene. *Res. Chem. Intermed.* **2015**, *41*, 5821–5837. [CrossRef]

39. Ema, K.; Hibino, Y.; Shigekawa, H.; Hyodo, S.-I. Component assignments of the Raman spectrum from highly elongated silica glass filbers. *Jpn. J. Appl. Phys.* **1987**, *26*, 649. [CrossRef]
40. Richet, P.; Mysen, B.O. High-temperature dynamics in cristobalite (SiO_2) and carnegieite ($NaAlSiO_4$): A raman spectroscopy study. *Geophys. Res. Lett.* **1999**, *26*, 2283–2286. [CrossRef]
41. Mysen, B.O.; Virgo, D.; Scarfe, C.M. Relations between the anionic structure and viscosity of silicate melts—A Raman spectroscopic study. *Am. Mineral.* **1980**, *65*, 690–710.
42. McMillan, P.F.; Wolf, G.H.; Poe, B.T. Vibrational spectroscopy of silicate liquids and glasses. *Chem. Geol.* **1992**, *96*, 351–366. [CrossRef]
43. Salazar Hoyos, L.A.; Faroldi, B.M.; Cornaglia, L.M. K-doping effect in the kinetics of CO_2 capture at high temperature over lithium silicates obtained from rice husks: In situ/operando techniques. *Ceram. Int.* **2021**, *47*, 1558–1570. [CrossRef]